Large-Scale Distribution of Arrival Directions of Cosmic Rays Detected at the the Pierre Auger Observatory Above 10^{16} eV

Olivier Deligny[1], for the Pierre Auger Collaboration

[1] IPN Orsay, CNRS/IN2P3 & Université Paris Sud

[2] full author list: http://www.auger.org/archive/authors_2013_05.html

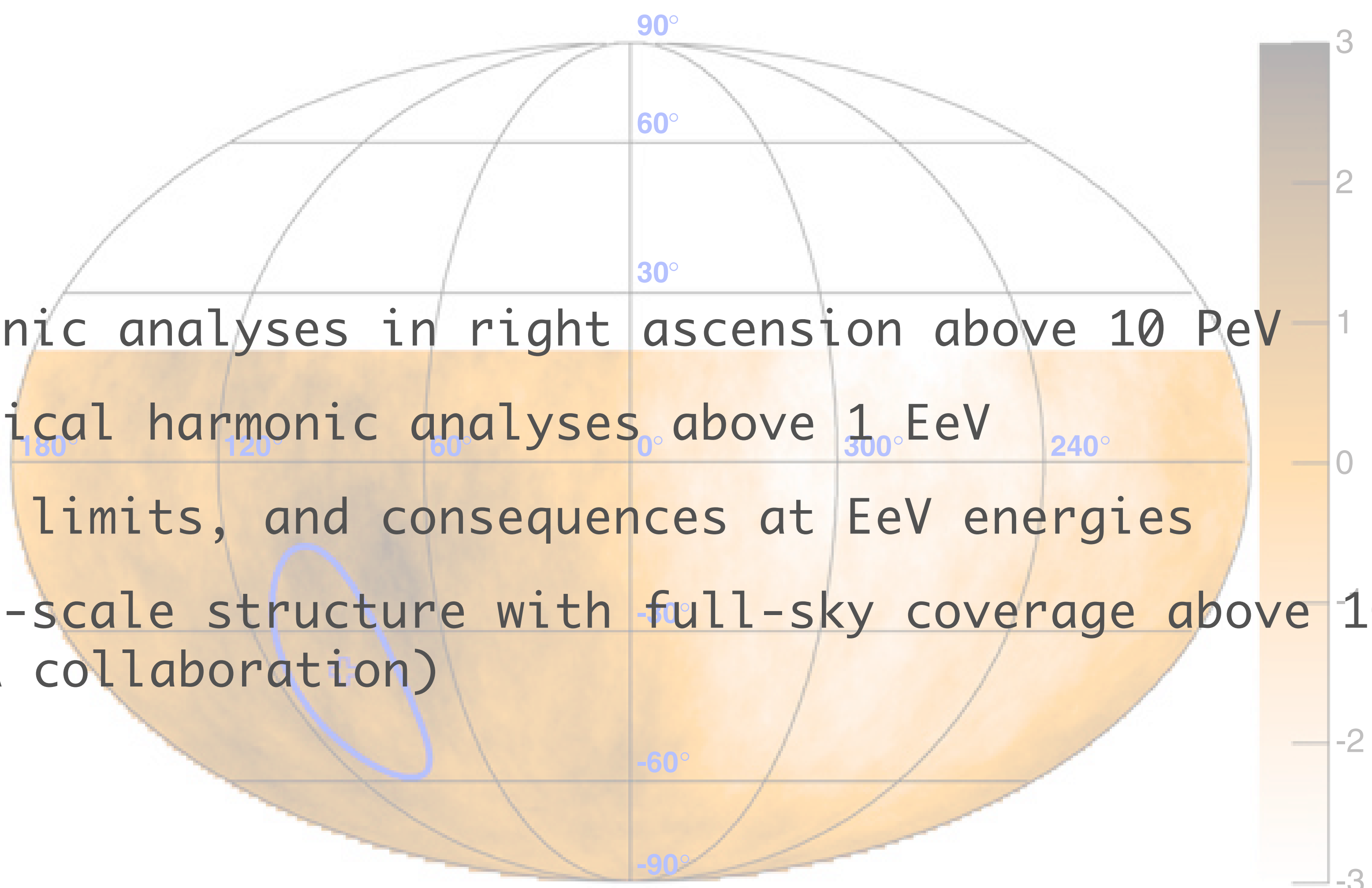

1. Harmonic analyses in right ascension above 10 PeV
2. Spherical harmonic analyses above 1 EeV
3. Upper limits, and consequences at EeV energies
4. Large-scale structure with full-sky coverage above 10 EeV (with TA collaboration)

Cosmic Ray Anisotropy Workshop, Madison, September 2013

0. The Pierre Auger Observatory

- Designed to study Ultra High Energy Cosmic Rays ($E > 10^{18}$ eV)
- Located near Malargüe, in Argentina

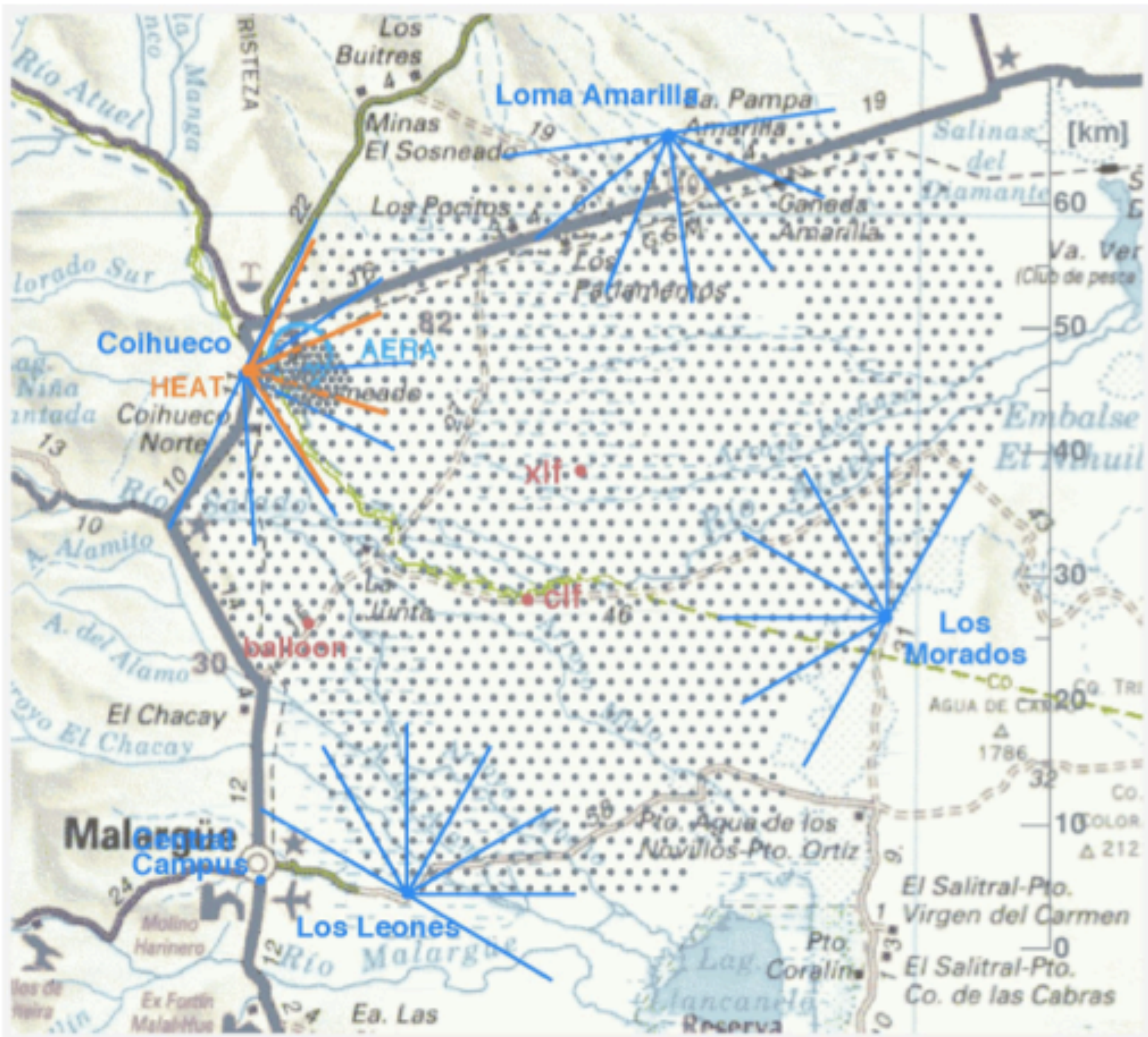

Hybrid detection of UHECR:

- Surface Detector (SD): 1600 water-Cherenkov detectors covering 3000 km^2 on a triangular grid with 1500 m spacing
- Infill detectors with 750 m spacing (23.5 km^2 area) enhancing the Observatory capabilities down to 10^{16} eV (full efficiency @ 3×10^{17} eV)
- Fluorescence Detector (FD): 27 fluorescence telescopes at 4 sites overlooking the SD array

1. First Harmonic Analyses in RA

➡ Astropart. Phys. 34 (2011) 628
(updated at last ICRC)

Harmonic expansion of the angular distribution in α :

$$\Phi(\alpha) = a_0 + \sum_{n>0} a_n^c \cos n\alpha + \sum_{n>0} a_n^s \sin n\alpha.$$

• For a directional exposure function ω(α), recovering of the Fourier coefficients through:

$$\overline{a}_n^c = \frac{2}{\widetilde{N}} \sum_{1\leqslant i\leqslant N} \frac{\cos n\alpha_i}{\omega(\alpha_i)},$$

$$\overline{a}_n^s = \frac{2}{\widetilde{N}} \sum_{1\leqslant i\leqslant N} \frac{\sin n\alpha_i}{\omega(\alpha_i)},$$

with $\widetilde{N} = \sum_i 1/\omega(\alpha_i)$

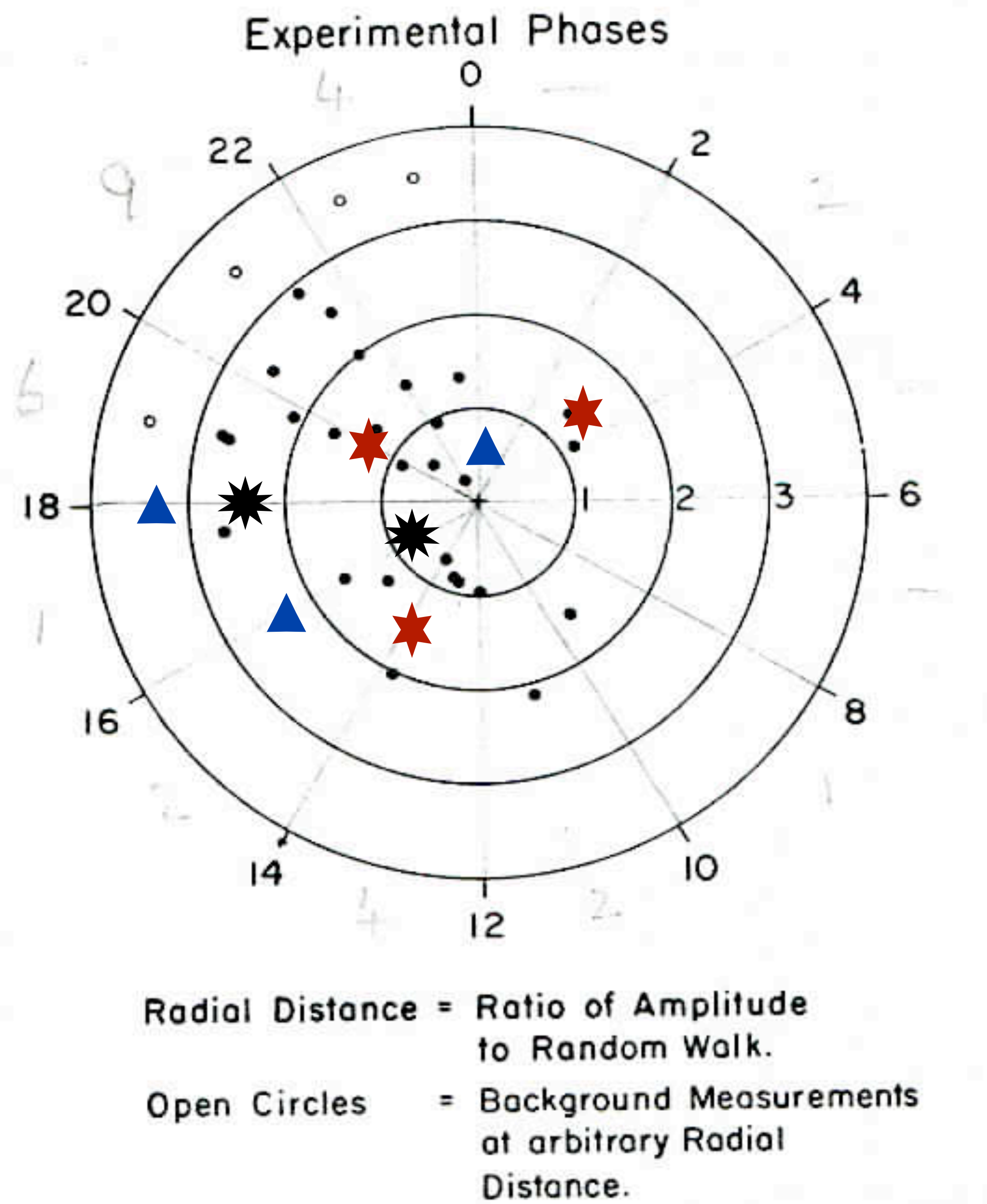

➡ Additional challenge : control of the event rate

Weather Effects and Large-Scale Analyses

➡ Astropart. Phys. 32 (2009) 89

- Changes of atmospheric conditions are known to influence the lateral extension of the showers ⇒ Modulations of the event rate vs time
- Above full efficiency, corrections of the energy estimator to (ρ,P) reference values allow us to remove modulations of experimental origin
- But, <u>amplification</u> of the effects below full efficiency :

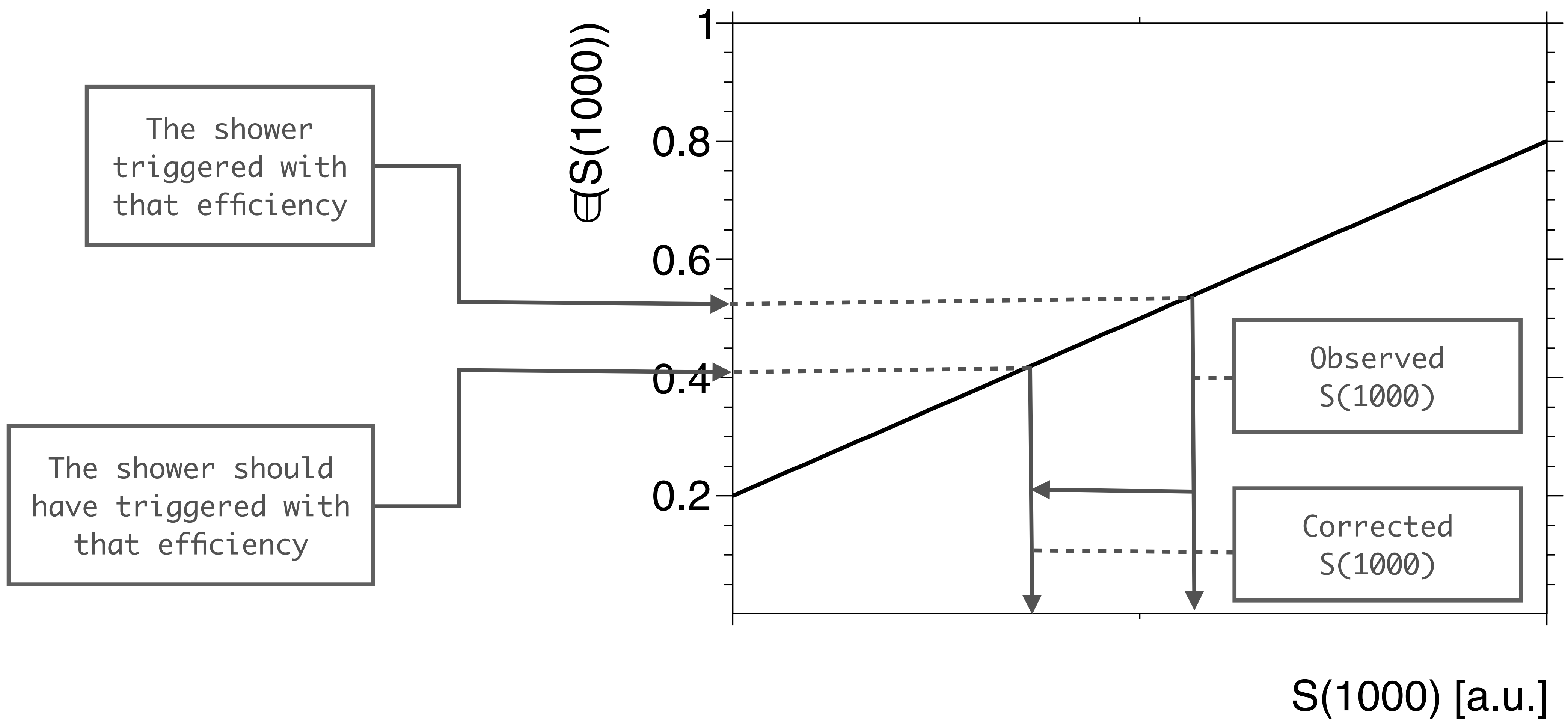

➡ Below full efficiency, use of the E/W method designed to subtract automatically spurious effects (though with reduced sensitivity) [ApJ 738 67 (2011)]

Spectral Analysis above 1 EeV

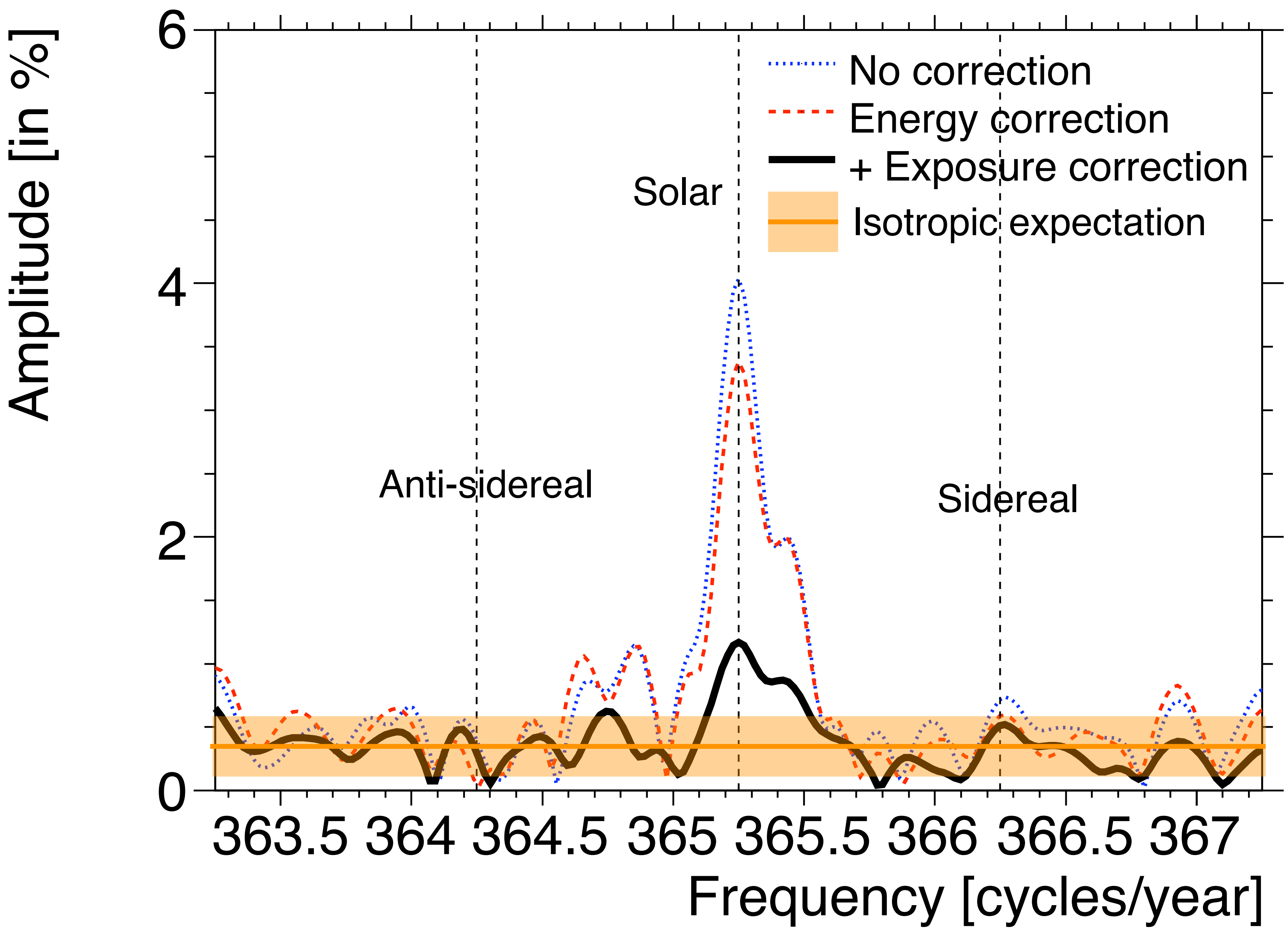

- Decoupling between frequencies clearly observed
- Amplitudes of random frequencies within noise
- Spurious sideband effect proportional to the solar amplitude: important to correct this frequency

Amplitude of the First Harmonic

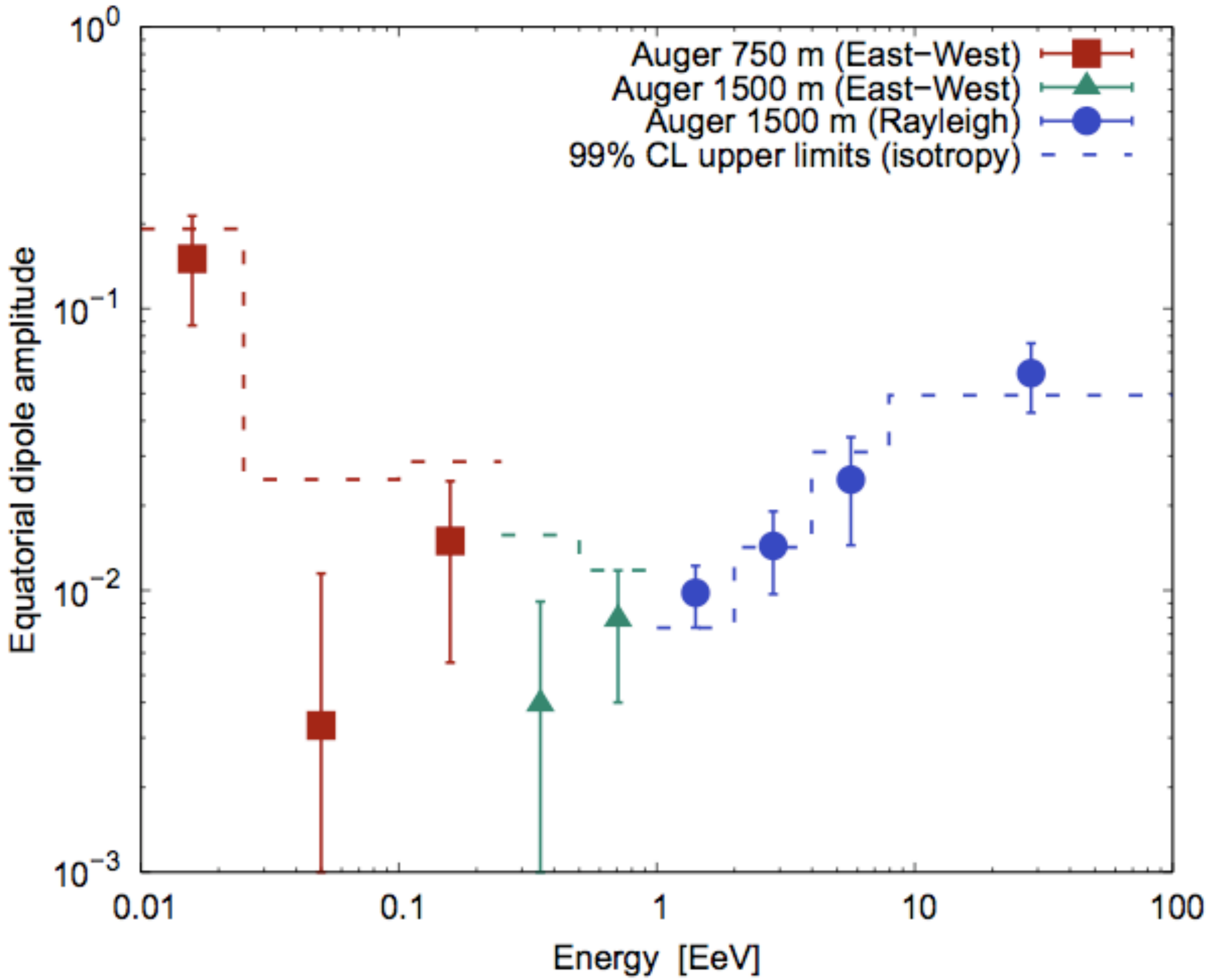

- r depends on the Observatory latitude and observed zenith angles
- To compare between experiments we use the equatorial dipole component $d_\perp \simeq r/\langle\cos\delta\rangle$

3 bins above 1 EeV have low probability to arise from isotropy

Phase vs Amplitude

Pure isotropy

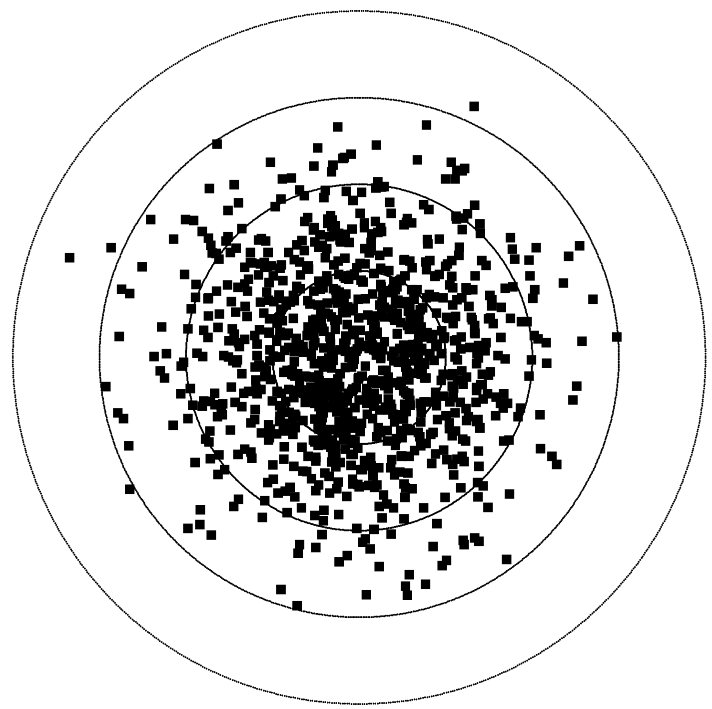

Almost isotropy
(signal size = mean noise)

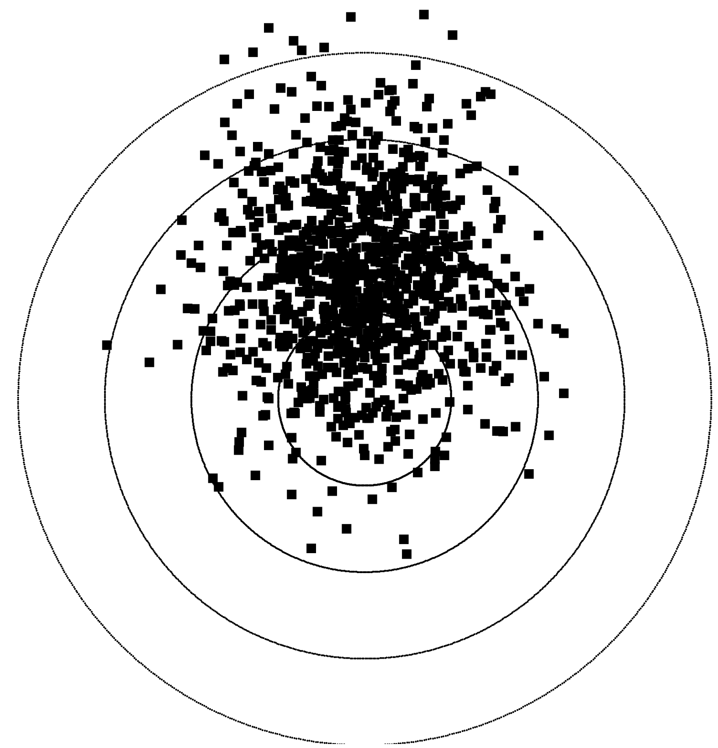

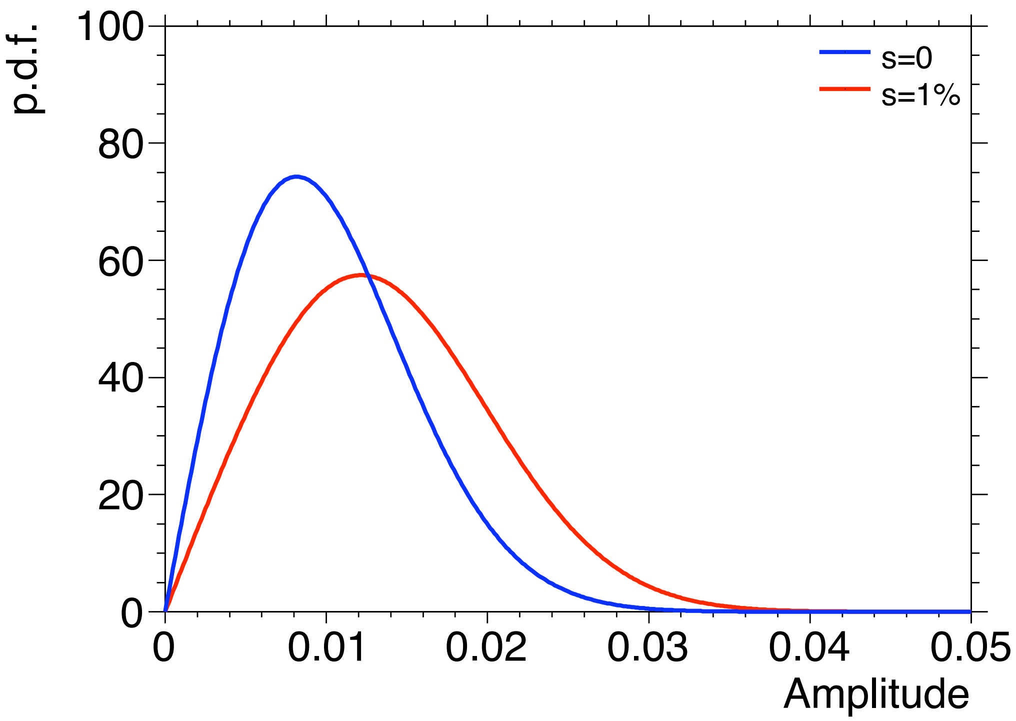

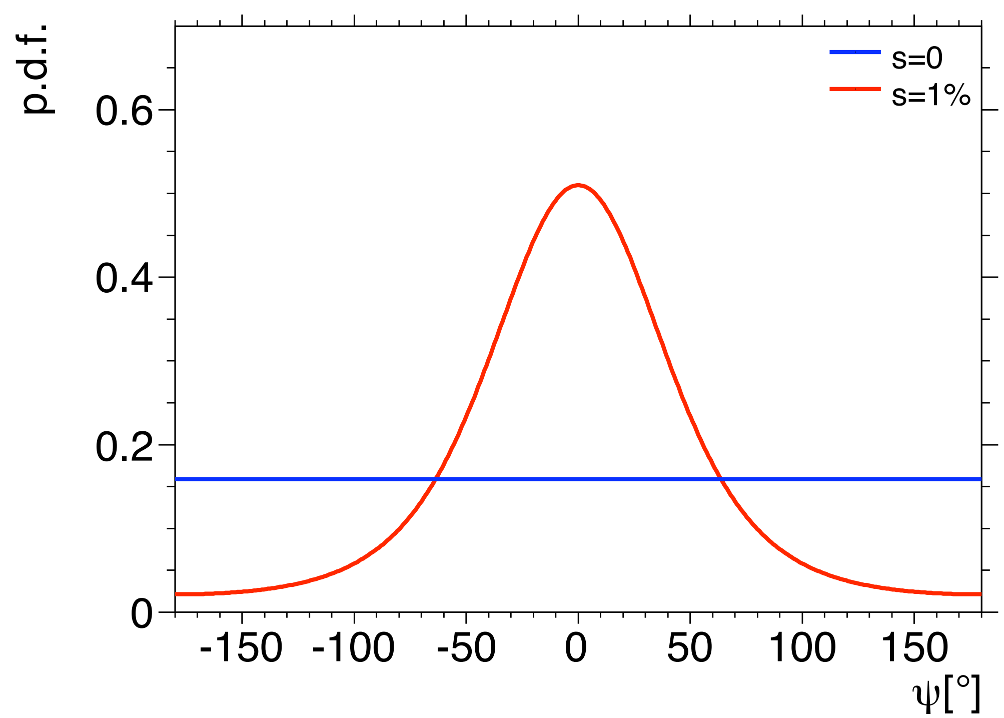

Phase vs Amplitude : Detection Power

Test on the phase for N_b bins

- LL ratio method: $L_0 = \prod_{i=1}^{i=N_b} p_{\rm iso}(\phi_i), \qquad L_1 = \prod_{i=1}^{i=N_b} p_{\Phi}(\phi_i) \rightarrow \lambda = \frac{L_0}{L_1}$
- $-2\ln(\lambda)$ pdf have to be computed
- $p = \int_{-2\ln(\lambda)_{\rm MC}}^{\infty} {\rm pdf}(-2\ln\lambda)$

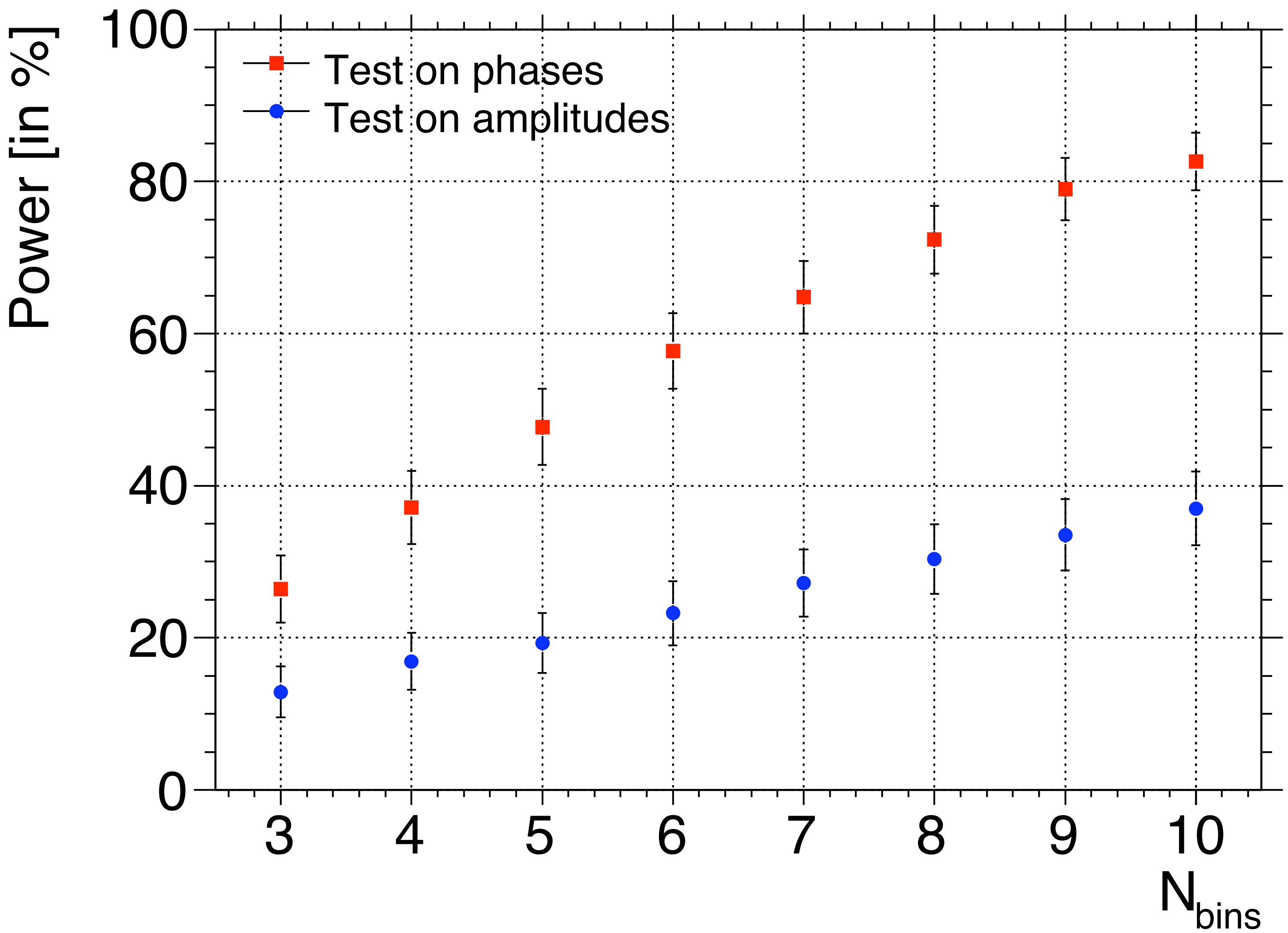

➡ Phase test ≈2.5 times more efficient

➡ A consistency of the phase measurement in adjacent energy intervals is thus expected with lower statistics than that required for the amplitude to significantly stand out from the background noise

Phase of the First Harmonic

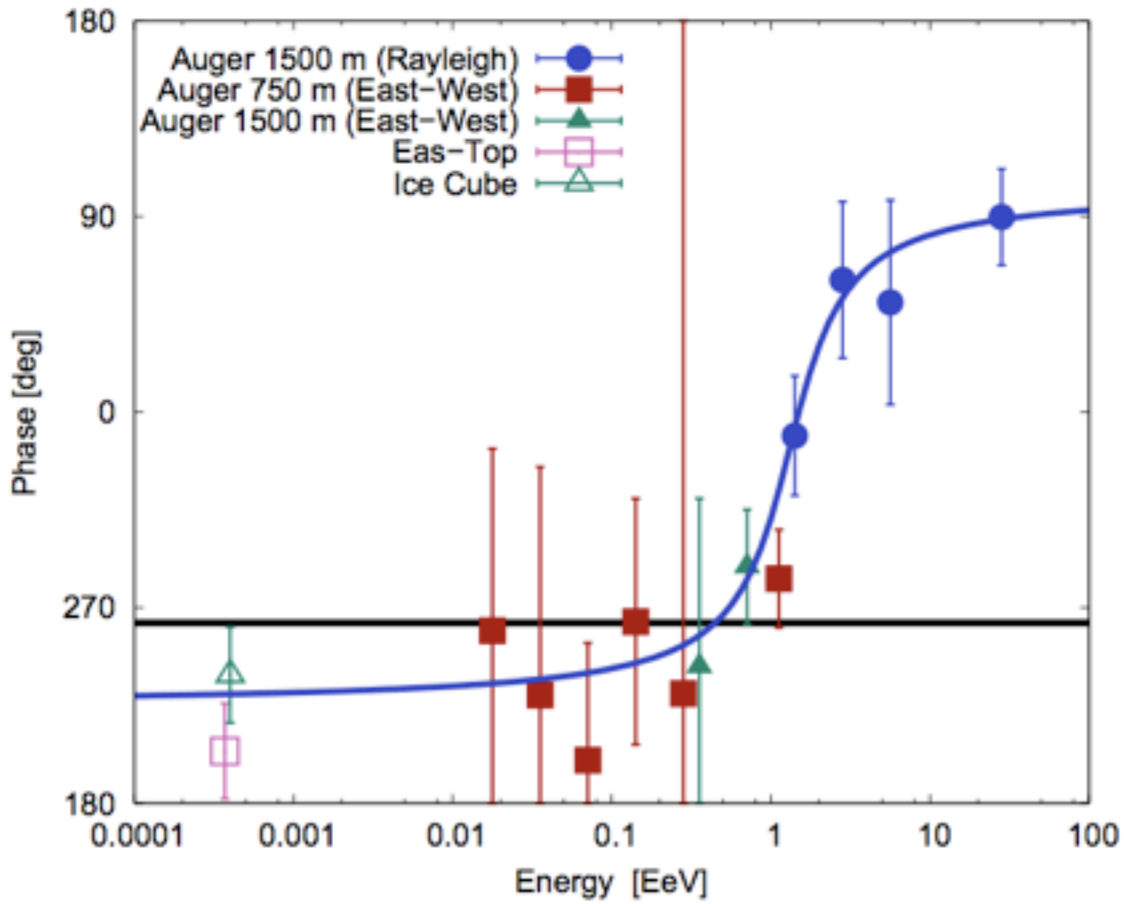

Eas-Top: M. Aglietta *et al.* 2009 ApJ **692** L130
IceCube: R. Abbasi *et al.* 2012 ApJ **746** 33

Infill data until April 2011
E = 0.01-2 EeV
Constant line fit
$\alpha \simeq 263^\circ \pm 19^\circ$

Prescription to check with new data at 99% CL:

- Started on the 25 of June 2011
- Constancy of phase at E<1 EeV with the Infill data
- Transition in phase at high energies

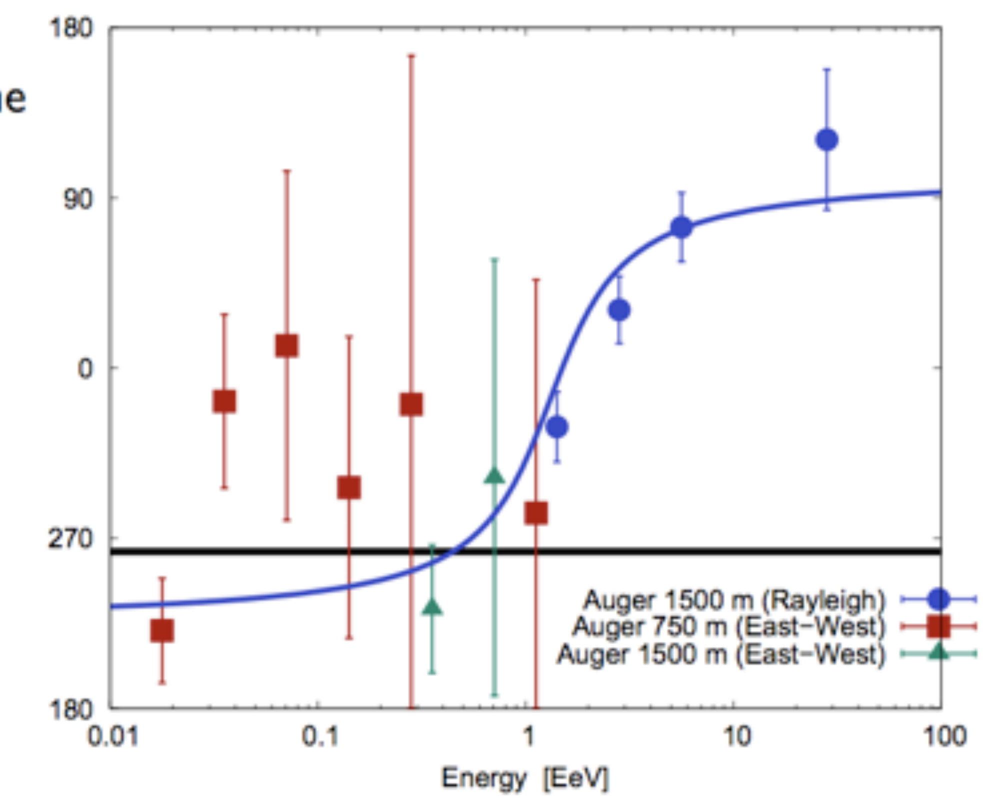

Phase of the first harmonic with events from 25 June 2011 to 31 December 2012.

2. Spherical Harmonic Analyses in RA/DEC

➡ ApJS 203 34 (2012)

(updated at last ICRC)

Expansion in Spherical Harmonics

$$\Phi(\mathbf{n}) = \sum_{\ell \geq 0} \sum_{m=-\ell}^{\ell} a_{\ell m} Y_{\ell m}(\mathbf{n}).$$

- Any anisotropy fingerprint is encoded in the set of spherical harmonics coefficients
- Non-zero ℓ modes arise from variations of the flux on an angular scale $\sim 1/\ell$ radians
- Dipole vector and quadrupole tensor of special interest, but the full set of moments is relevant

Partial-Sky Coverage

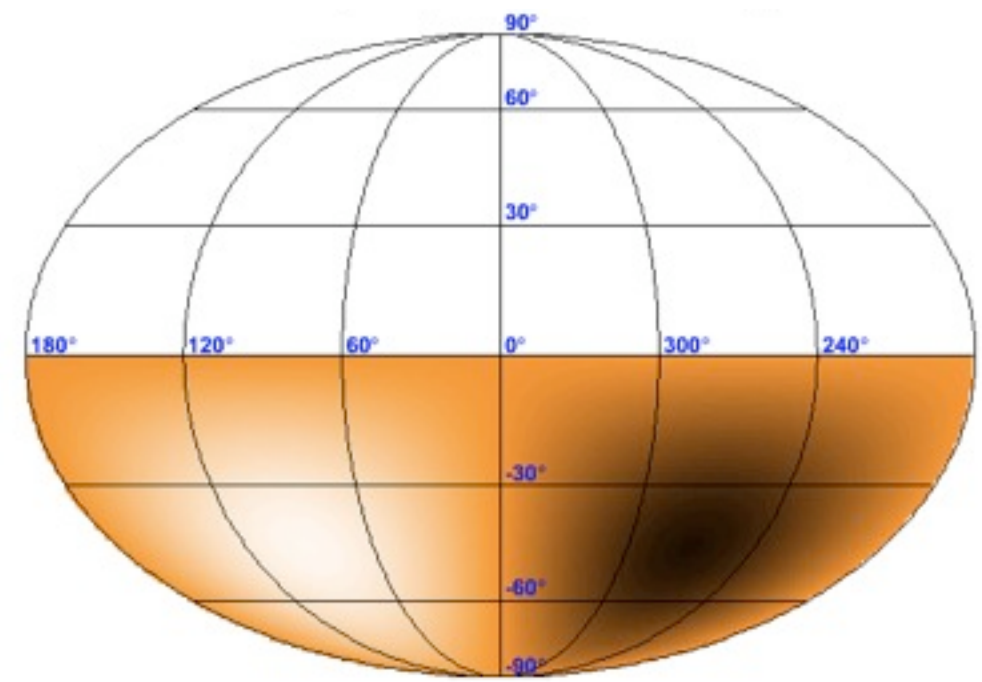

- Estimation possible only by assuming an upper bound L to the expansion in spherical harmonics
- Resolution degraded in proportion to exp(L) !

Control of the Event Rate

➡ JCAP 11 (2011) 022

- Influence of the geomagnetic field on the muons of the showers: distortions of the density of particles in the shower plane
- Dependence on local angles, inducing spurious anisotropies in declination δ

➡ Correction of the energy estimator to control the event rate

➡ Essential to search for anisotropies in δ !

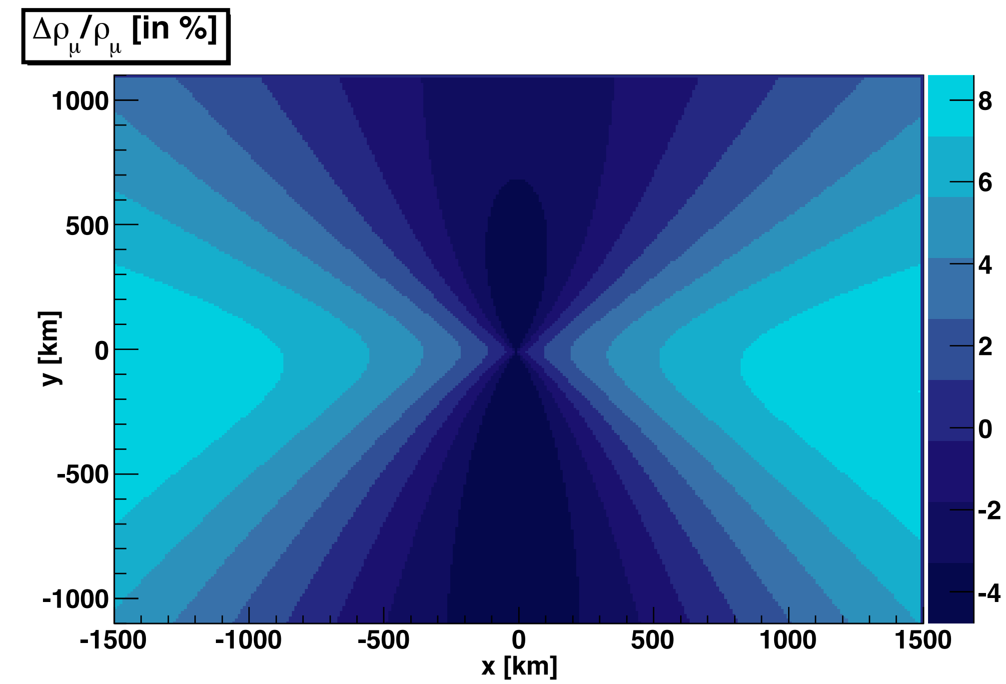

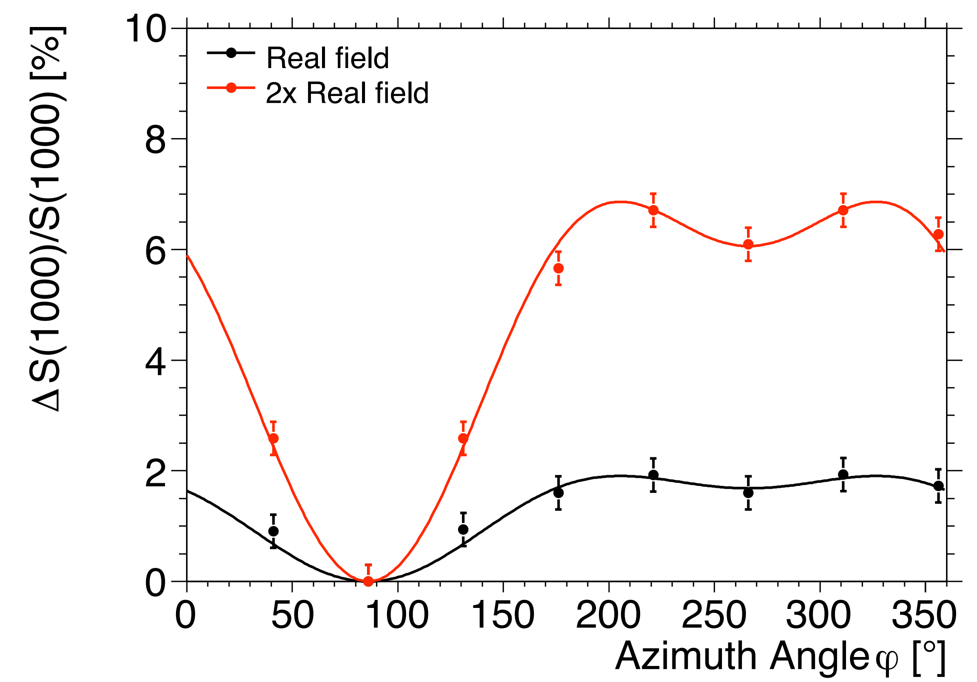

Directional Exposure

➡ Crucial ingredient to characterise the angular distribution in both α and δ

➡ Many additional effects w.r.t. ω(α) only

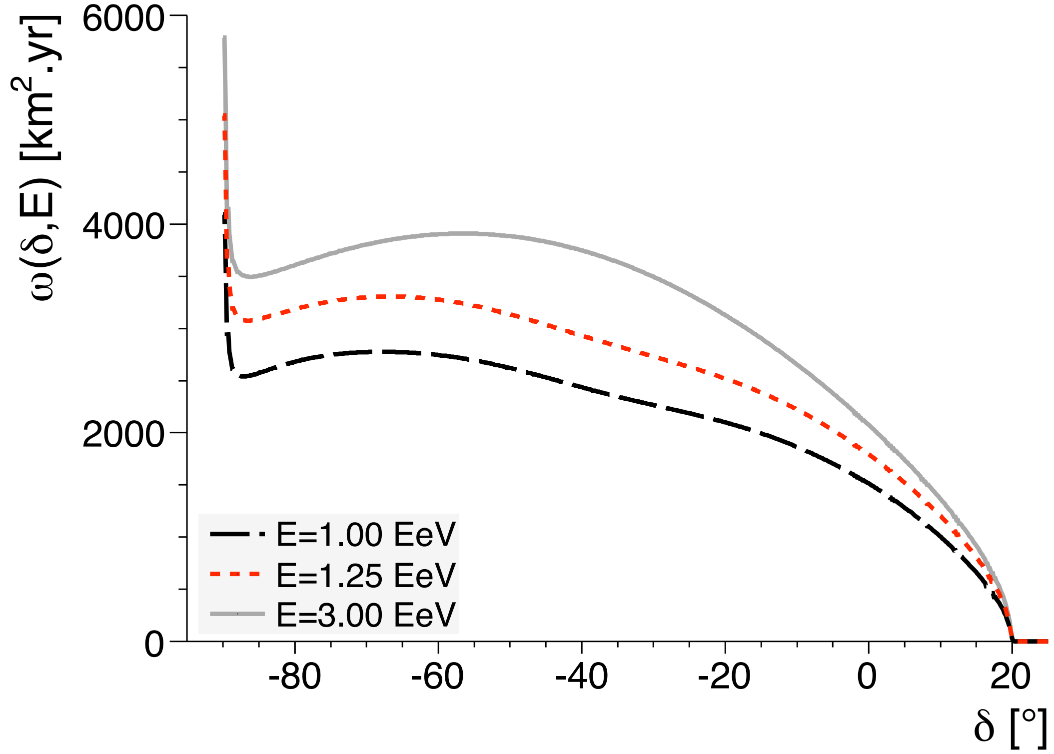

$$\omega(\delta, E) = \sum_{i=1}^{n_{\mathrm{cell}}} x^{(i)} \int_0^{24h} \mathrm{d}\alpha' \, a_{\mathrm{cell}}^{(i)}(\theta, \varphi) \, \left[\epsilon(\theta, \varphi, E) + \Delta\epsilon_{\mathrm{tilt}}(\theta, \varphi, E) \right]$$

on-time of each elemental cell (hexagon), in sidereal days

geometric directional aperture of each elemental cell - depends on the tilt of the cell and its latitude

detection efficiency

variation of the detection efficiency due to the tilted SD array

Detection Efficiency

Relative change in zenith angles induced by a dipole :

$$\Delta(dN/d\sin^2\theta) = \frac{N_{0,\mathrm{dipole}}}{N_{0,\mathrm{iso}}}\sin\ell_{\mathrm{site}}\sin\delta_d\cos\theta,$$

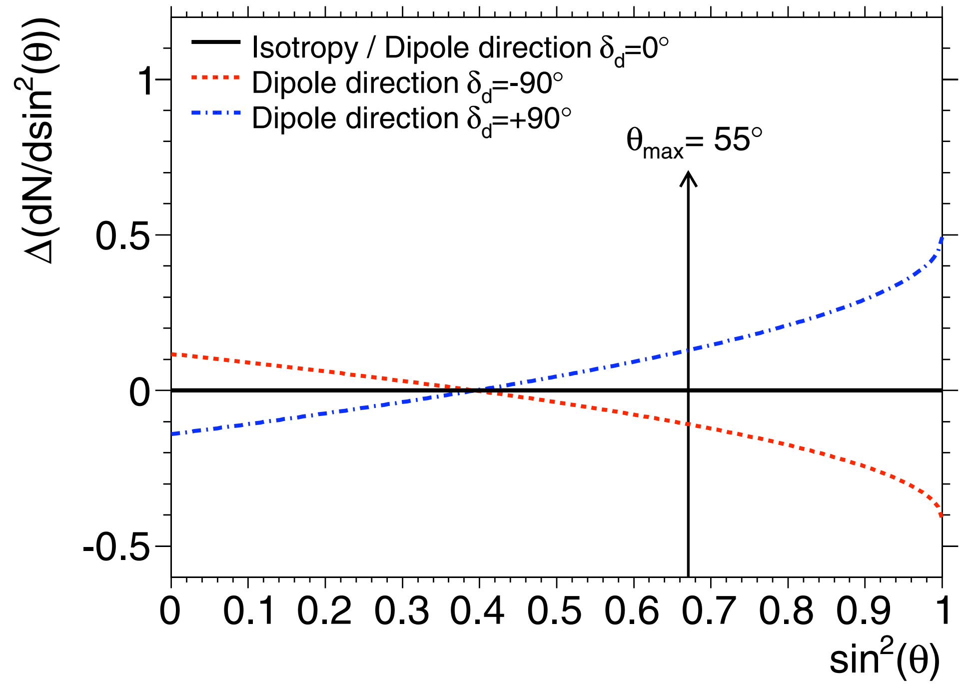

➡ <u>Empirical approach</u>, based on the quasi-invariance of the zenithal distribution to large scale anisotropies for ϑ<~60°

$$\langle\epsilon(\theta,\varphi,E)\rangle_\varphi = \frac{1}{\mathcal{N}}\frac{\mathrm{d}N(\sin^2(\theta),E)}{\mathrm{d}\sin^2(\theta)}$$

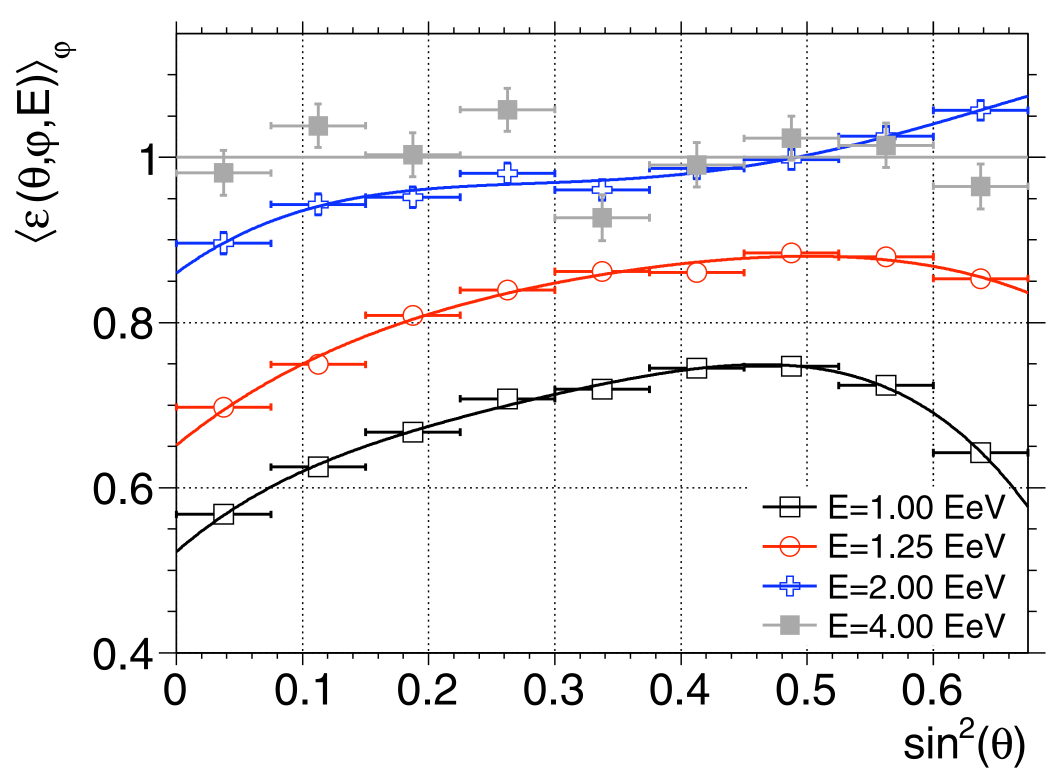

Geomagnetic Effects below Full Efficiency

- Same mechanism of modulation of detection efficiency as for weather effects
- Dominant source of modulation in azimuth of ε above 1 EeV
- From MC studies :

$$\begin{aligned}\epsilon(\theta,\varphi,E) &= \frac{1}{\mathcal{N}}\frac{\mathrm{d}N(\sin^2(\theta),E(1+\Delta(\theta,\varphi))^B)}{\mathrm{d}\sin^2(\theta)} \\ &\simeq \langle\epsilon(\theta,\varphi,E)\rangle_\varphi + \frac{BE\Delta(\theta,\varphi)}{\mathcal{N}}\frac{\partial\langle\epsilon(\theta,\varphi,E)\rangle_\varphi}{\partial E}.\end{aligned}$$

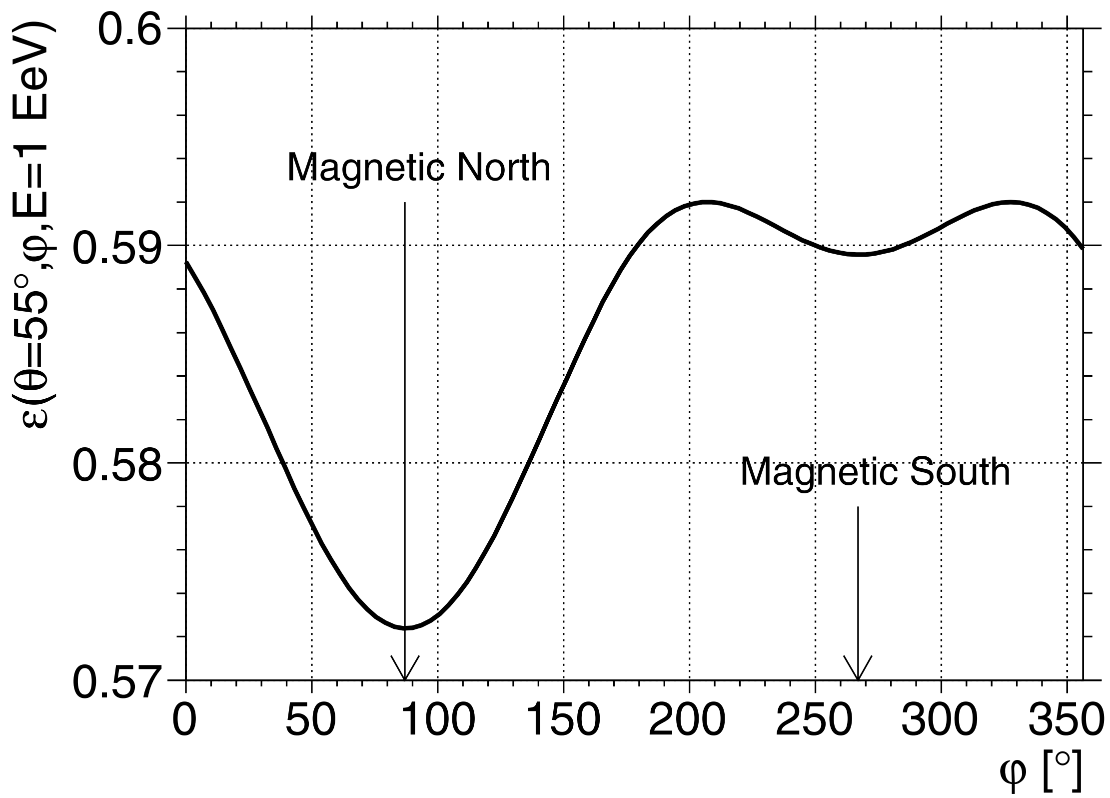

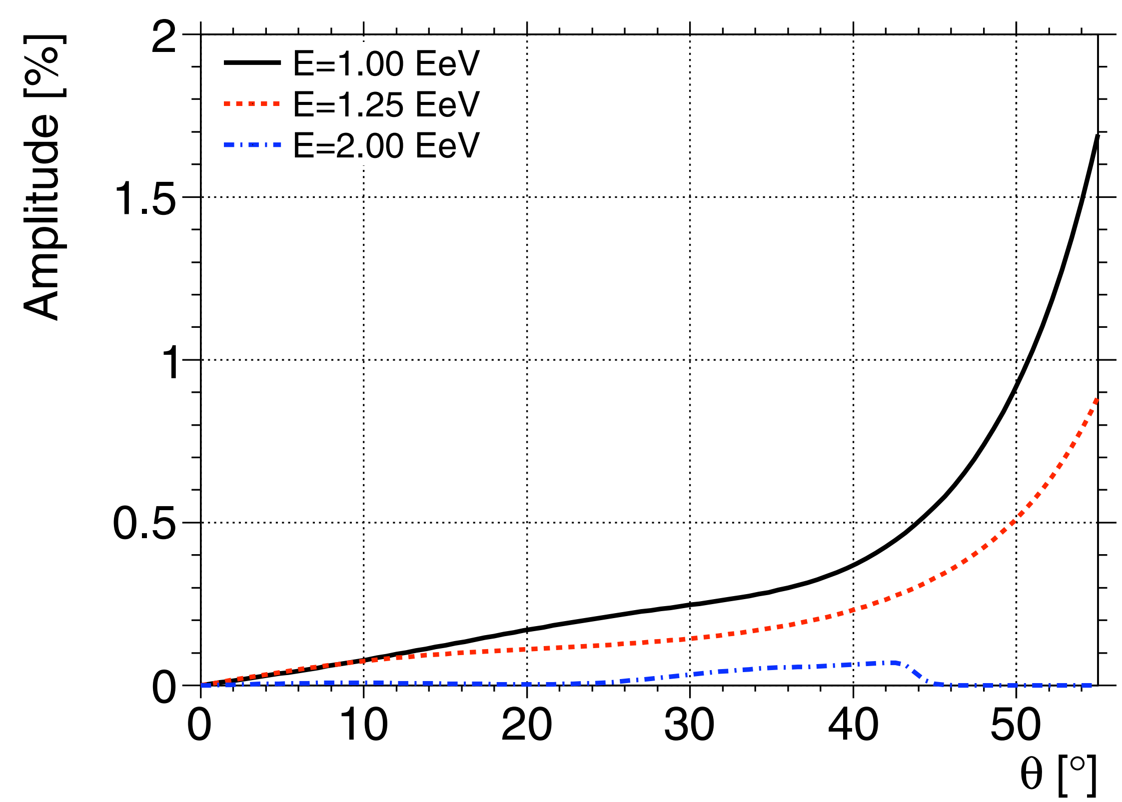

Tilt/Extension of the SD Array

- The tilt induces a change of the projected surface :

$$a_{\mathrm{cell}}^{(i)}(\theta, \varphi) = 1.95\,\mathbf{n} \cdot \mathbf{n}_{\perp}^{(\mathbf{i})} \simeq 1.95\left[1 + \zeta^{(i)} \tan\theta \cos\left(\varphi - \varphi_0^{(i)}\right)\right]\cos\theta$$

- Spatial extension of the array : explicit dependence of ϑ and φ on the latitude of the cell

- The tilt induces a variation of the detection efficiency below saturation :

$$\Delta\epsilon_{\mathrm{tilt}}(\theta, \varphi, E) = \frac{E^3\left(E_{0.5}^3 - E_{0.5}^{\mathrm{tilt}\,3}(\theta, \varphi)\right)}{\left(E^3 + E_{0.5}^3\right)\left(E^3 + E_{0.5}^{\mathrm{tilt}\,3}(\theta, \varphi)\right)}$$

$$E_{0.5}^{\mathrm{tilt}}(\theta, \varphi) \simeq E_{0.5} \times \left[1 + \zeta^{\mathrm{eff}} \tan\theta \cos\left(\varphi - \varphi_0^{\mathrm{eff}}\right)\right]^{3/2}$$

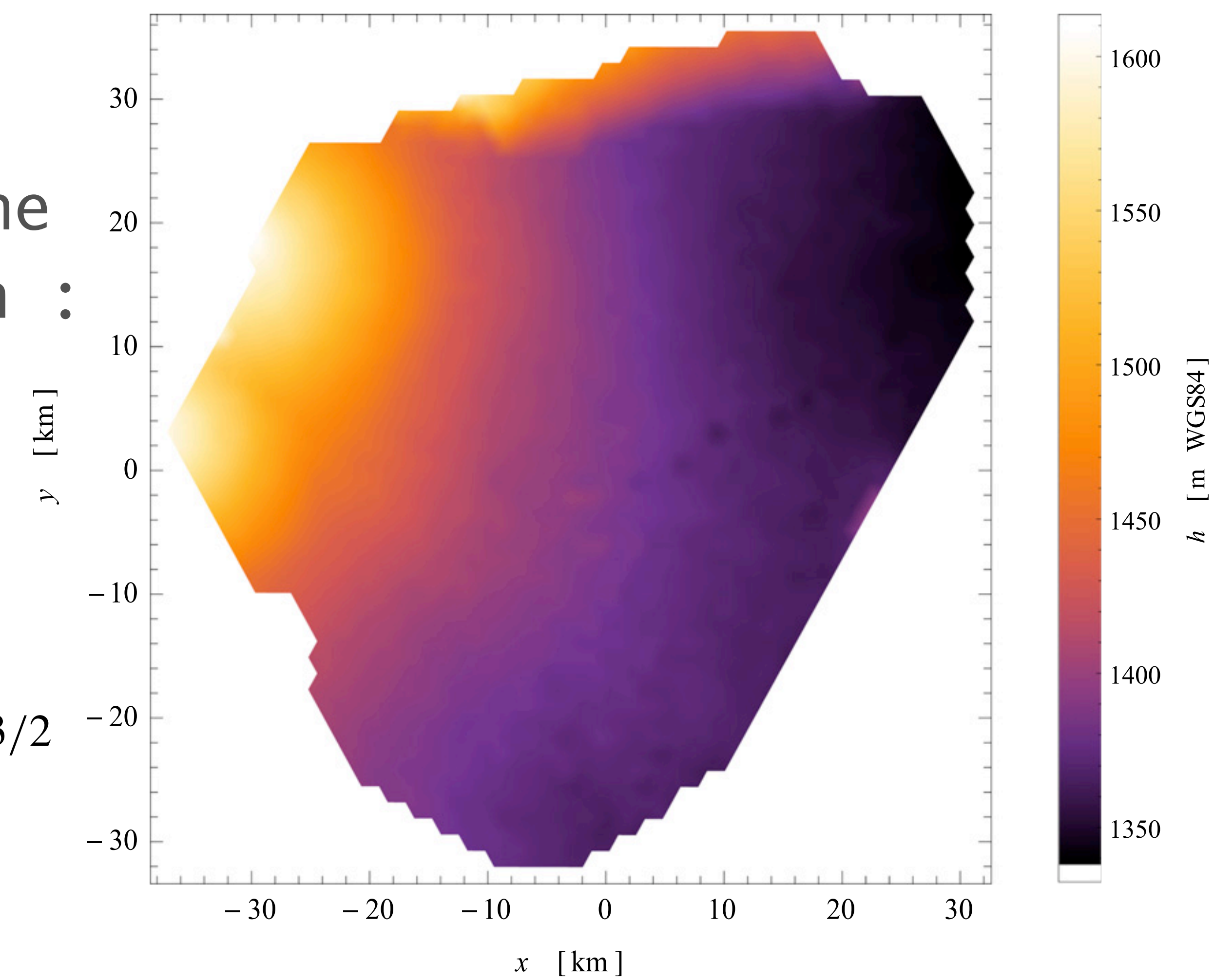

Recovering Multipolar Coefficients

Partial-Sky Coverage

$$
\begin{aligned}
b_{\ell m} &= \int_{\Delta\Omega} \mathrm{d}\Omega_{\mathbf{n}}\, \tilde{\omega}(\mathbf{n}, \Delta E)\Phi(\mathbf{n})\, Y_{\ell m}(\mathbf{n}) \\
&= \sum_{\ell' \geq 0} \sum_{m'=-\ell'}^{\ell'} a_{\ell' m'} \int_{\Delta\Omega} \mathrm{d}\Omega_{\mathbf{n}}\, \tilde{\omega}(\mathbf{n}, \Delta E)\, Y_{\ell' m'}(\mathbf{n})\, Y_{\ell m}(\mathbf{n}).
\end{aligned}
$$

→ multipolar moment as seen through the coverage

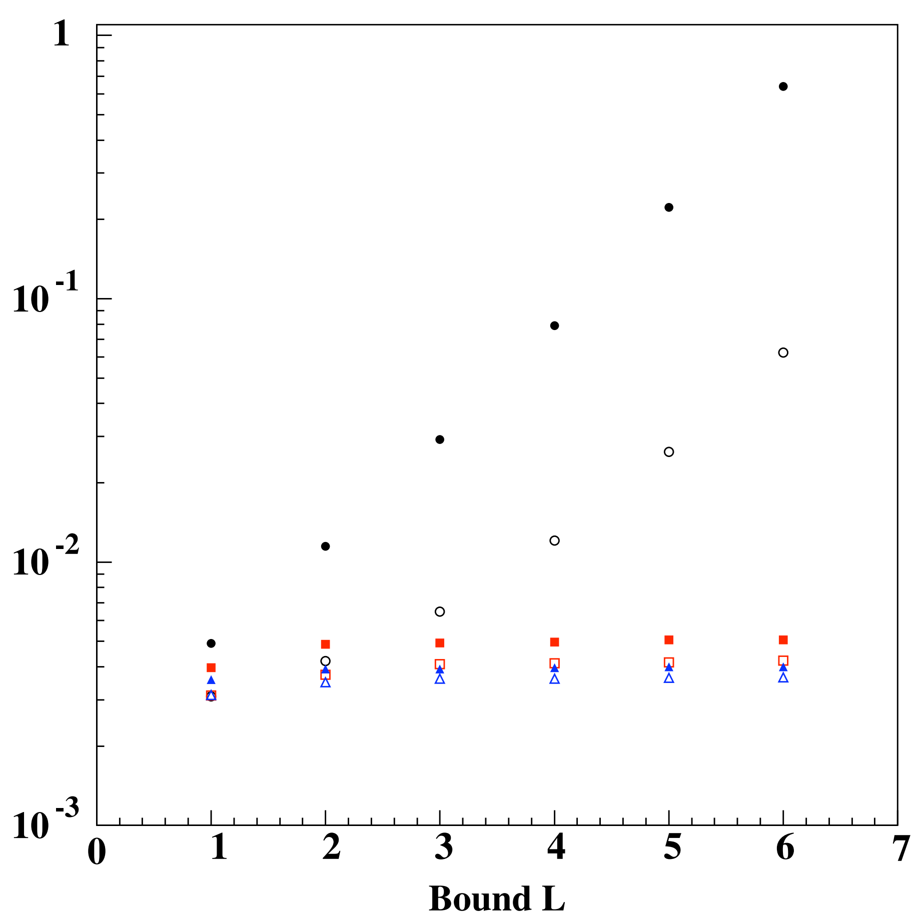

$$
\overline{a}_{\ell m} = \sum_{\ell'=0}^{\ell_{\max}} \sum_{m'=-\ell'}^{\ell'} [K_{\ell_{\max}}^{-1}]_{\ell m}^{\ell' m'} \overline{b}_{\ell' m'}.
$$

- Recovered coefficients meaningful if $\phi(n)$ bounded to some bound L
- BUT exponential degradation of the resolution each time the bound is incremented by 1

Dipole Analysis (L=1)

$$\Phi(\mathbf{n}) = \frac{\Phi_0}{4\pi}(1 + r\mathbf{d}\cdot\mathbf{n}),$$

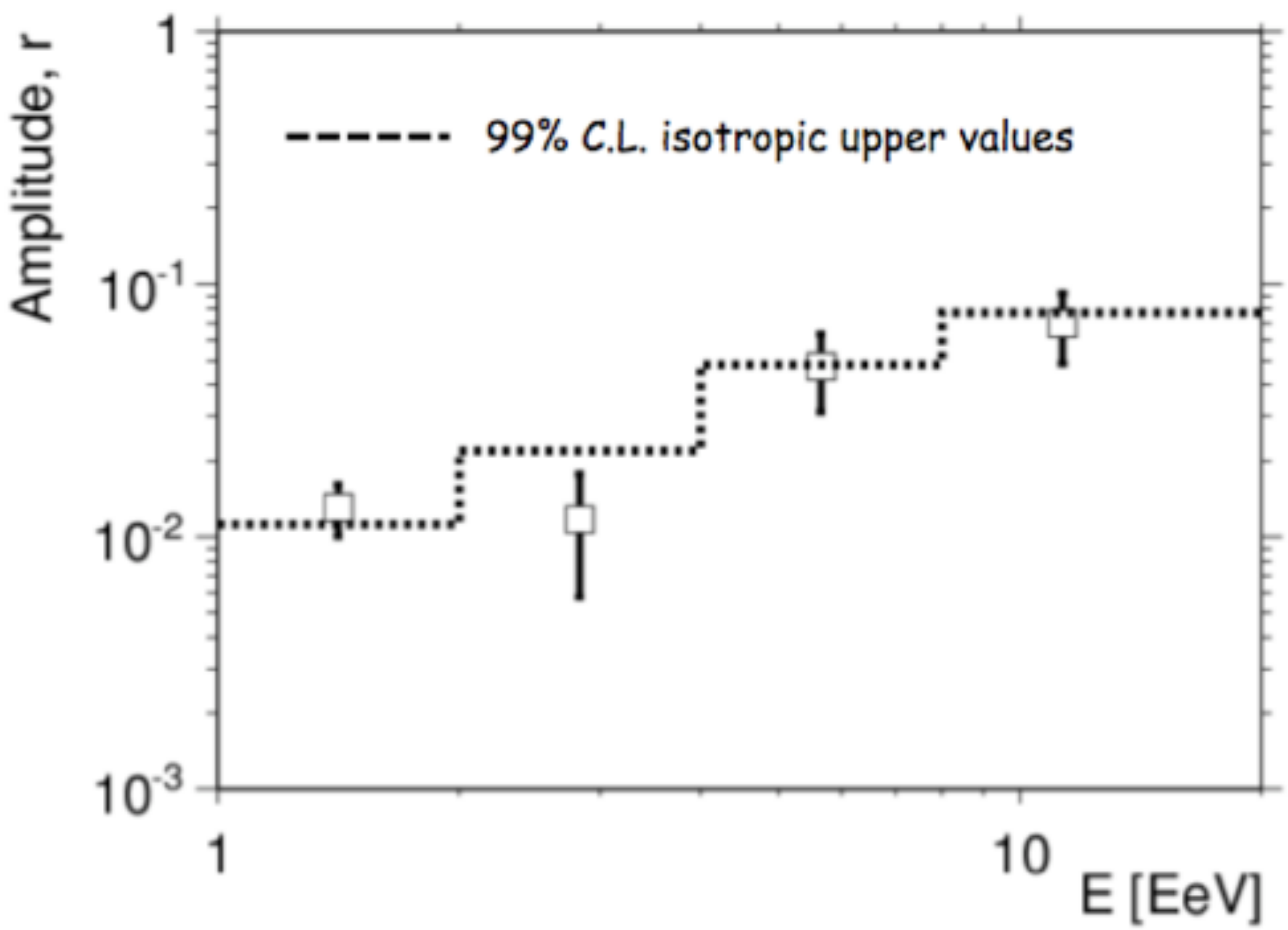

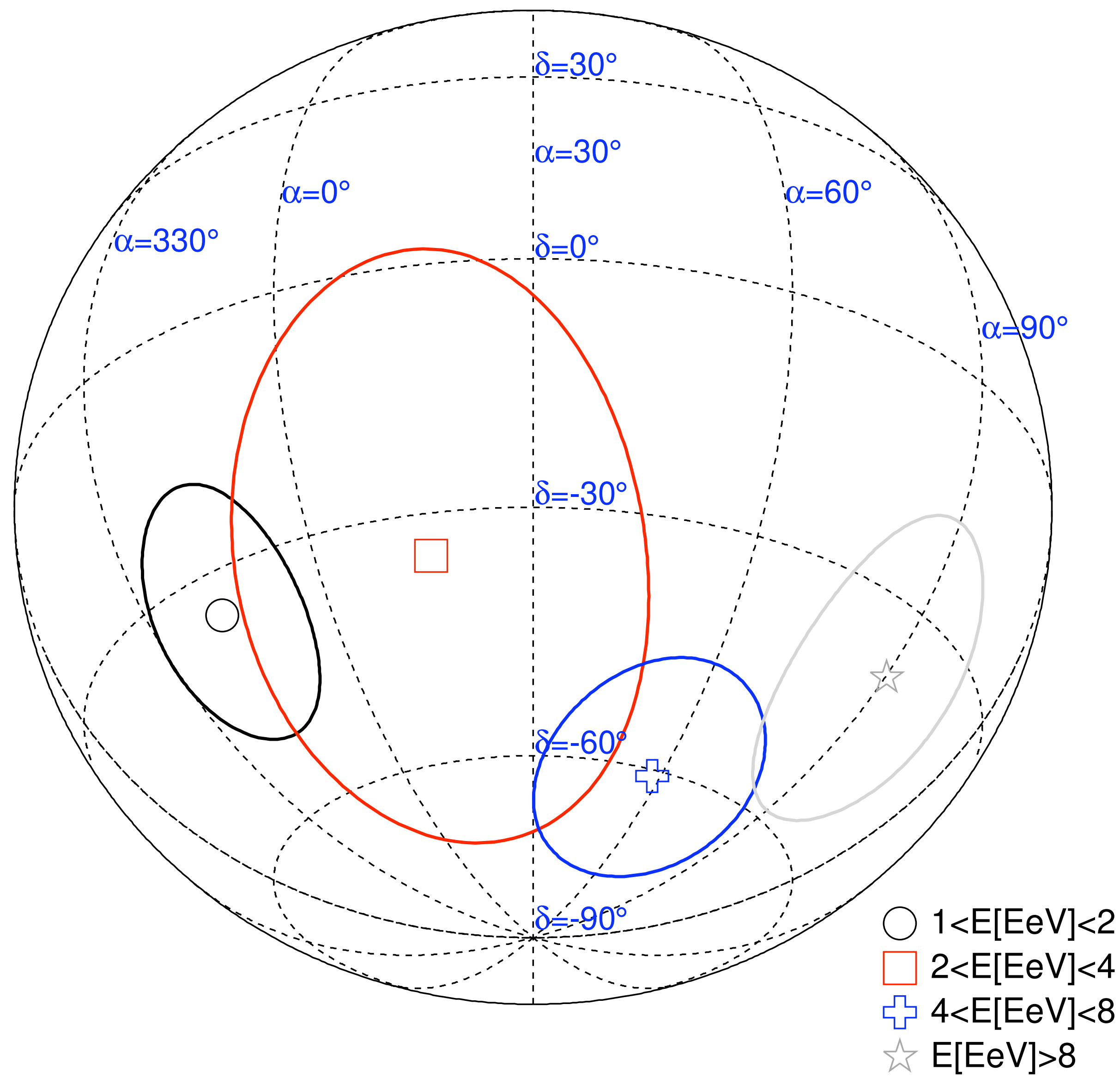

Quadrupole Analysis (L=2)

$$\Phi(\mathbf{n}) = \frac{\Phi_0}{4\pi}(1 + r\mathbf{d}\cdot\mathbf{n} + \lambda_+(\mathbf{q_+}\cdot\mathbf{n})^2 + \lambda_0(\mathbf{q_0}\cdot\mathbf{n})^2 + \lambda_-(\mathbf{q_-}\cdot\mathbf{n})^2).$$

$$\beta \equiv \frac{(\lambda_+ - \lambda_-)}{(2 + \lambda_+ + \lambda_-)} = \frac{\Phi_{max} - \Phi_{min}}{\Phi_{max} + \Phi_{min}}$$

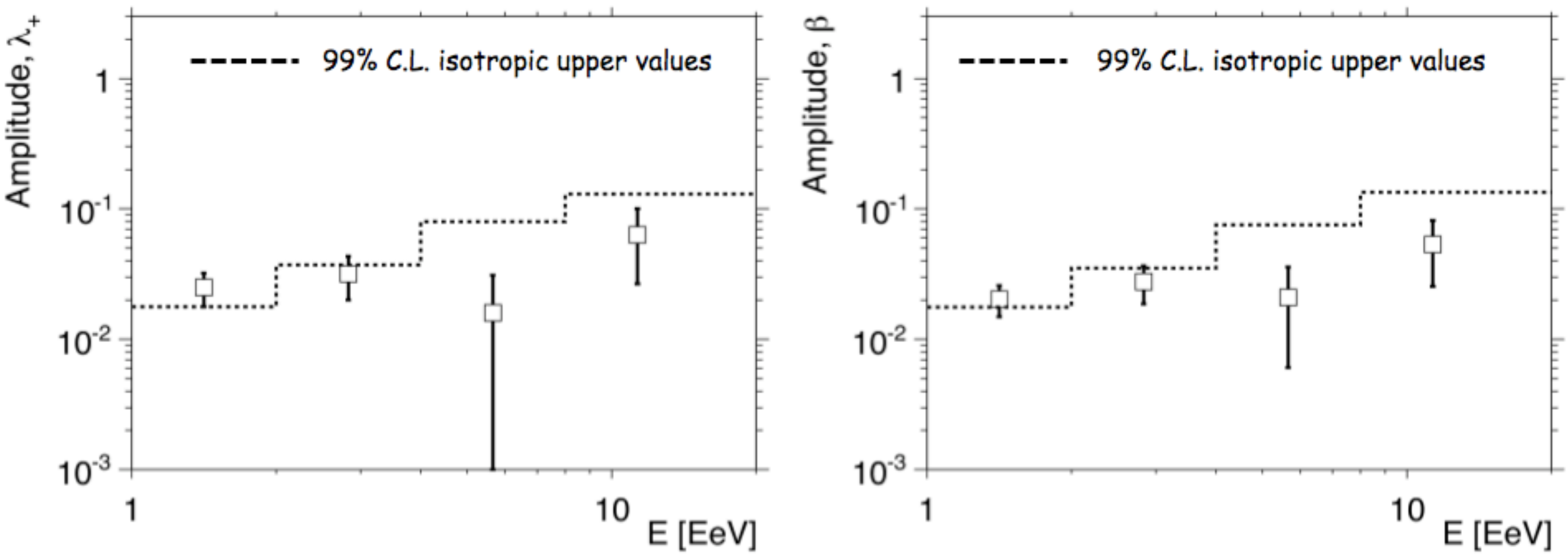

3. Upper Limits and Consequences

➡ ApJL 762 L13 (2013)
& ApJS 203 34 (2012)

Generic Estimate of Anisotropies from EeV-Galactic Stationary Sources

- Numerical integration of trajectories required in this energy range

➡ Back tracking of anti-particles with random directions from the Earth to outside the Galaxy [Thielheim & Langhoff, J.Phys.A,1,694 (1968)]

- Each particle probes the total luminosity along the path of propagation from each direction as seen from the Earth
- For stationary sources emitting equally in all directions, the time spent in the source region is proportional to the flux detected in that direction

Upper Limits and Consequences

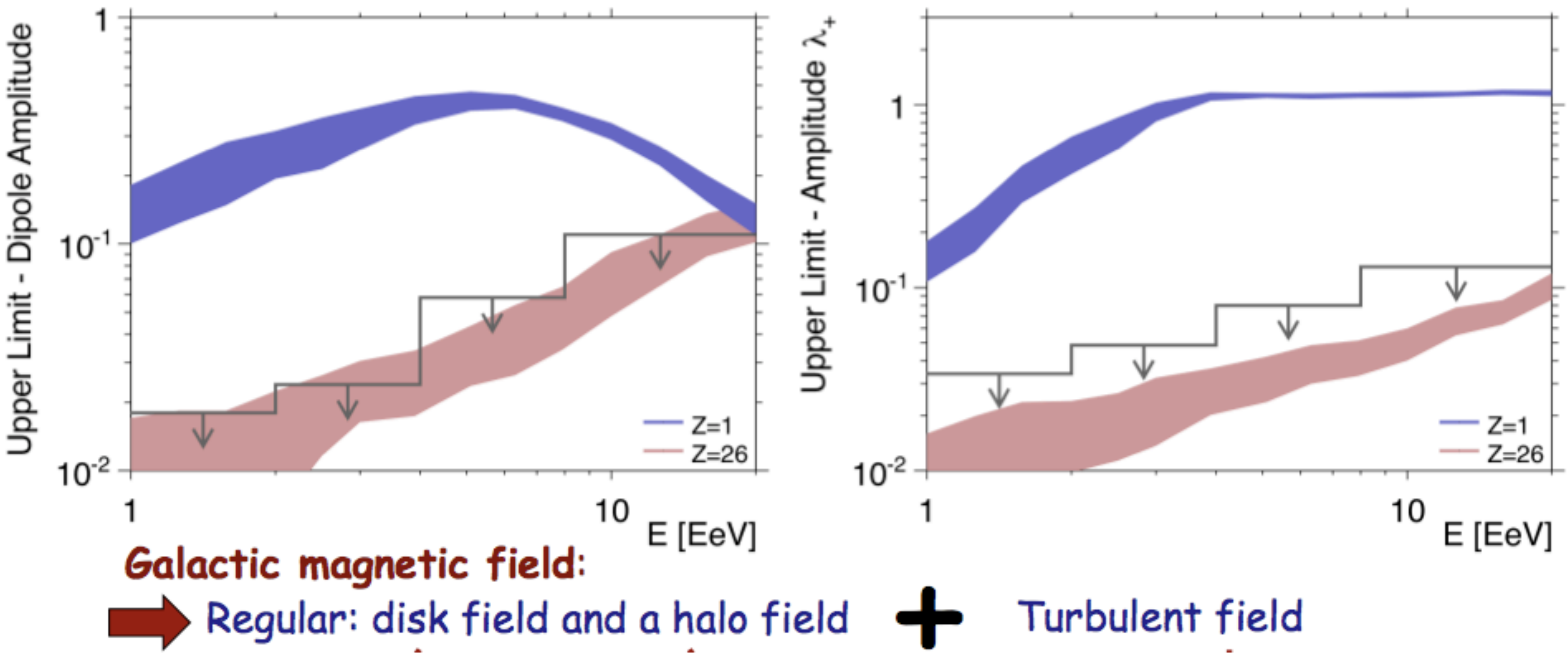

➡ While other magnetic field models, source distributions and emission assumptions must be considered before definitive conclusions can be drawn, the example considered here illustrates the potential power of these observational limits on the dipole anisotropy to exclude the hypothesis that the light component of cosmic rays is of Galactic origin.

4. Large-Scale Structure with Full-Sky Coverage

➡ Joint Auger/TA paper in preparation

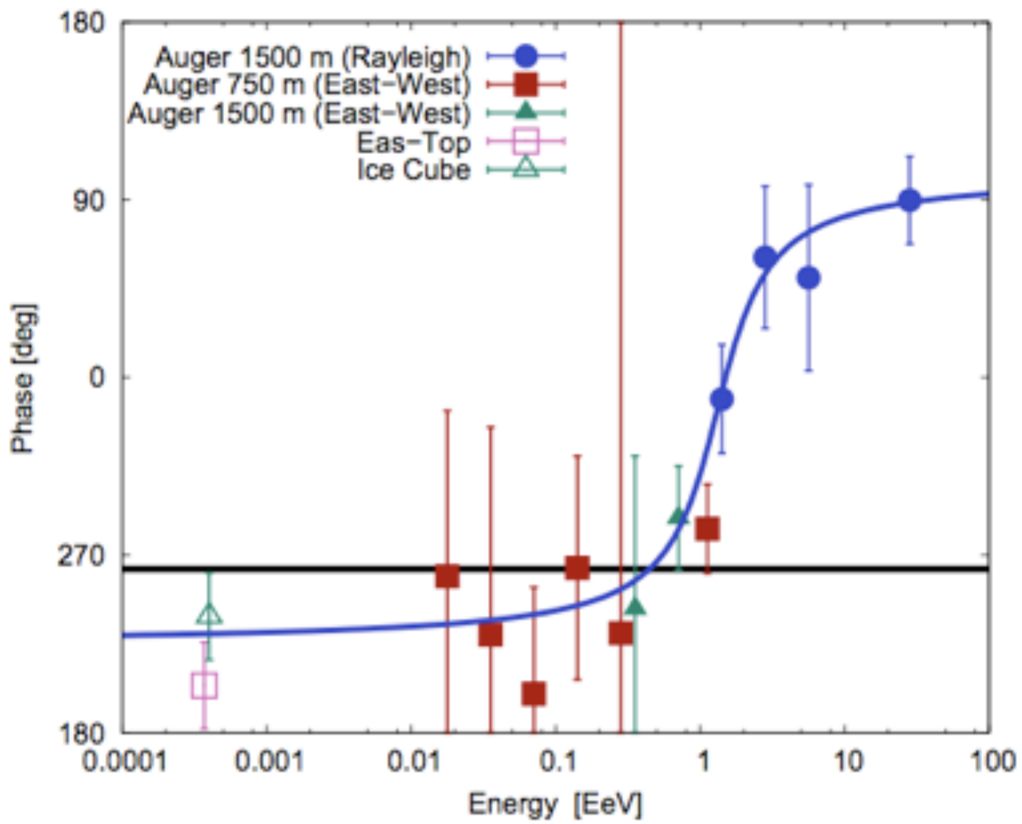

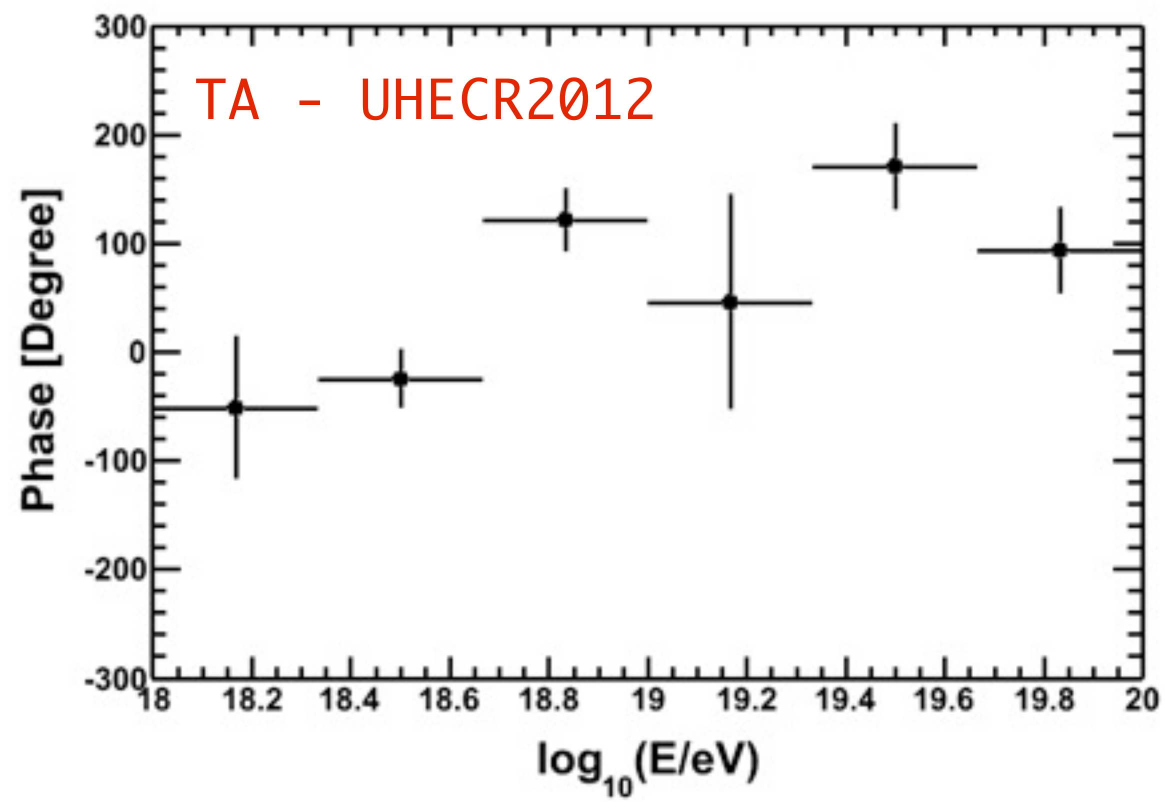

- Direction in right ascension consistent in both hemispheres
- Goal : anisotropy studies with combined Auger/TA data
- Many advantages with full-sky coverage in addition to the increased statistics (no need for an upper bound L)

Full-Sky Coverage

- Zenith ranges :[0-55°] for TA, [0-60°] for Auger

➡ Zenith ranges + latitudes : full-sky coverage achieved

- Energy threshold : geometric directional exposure

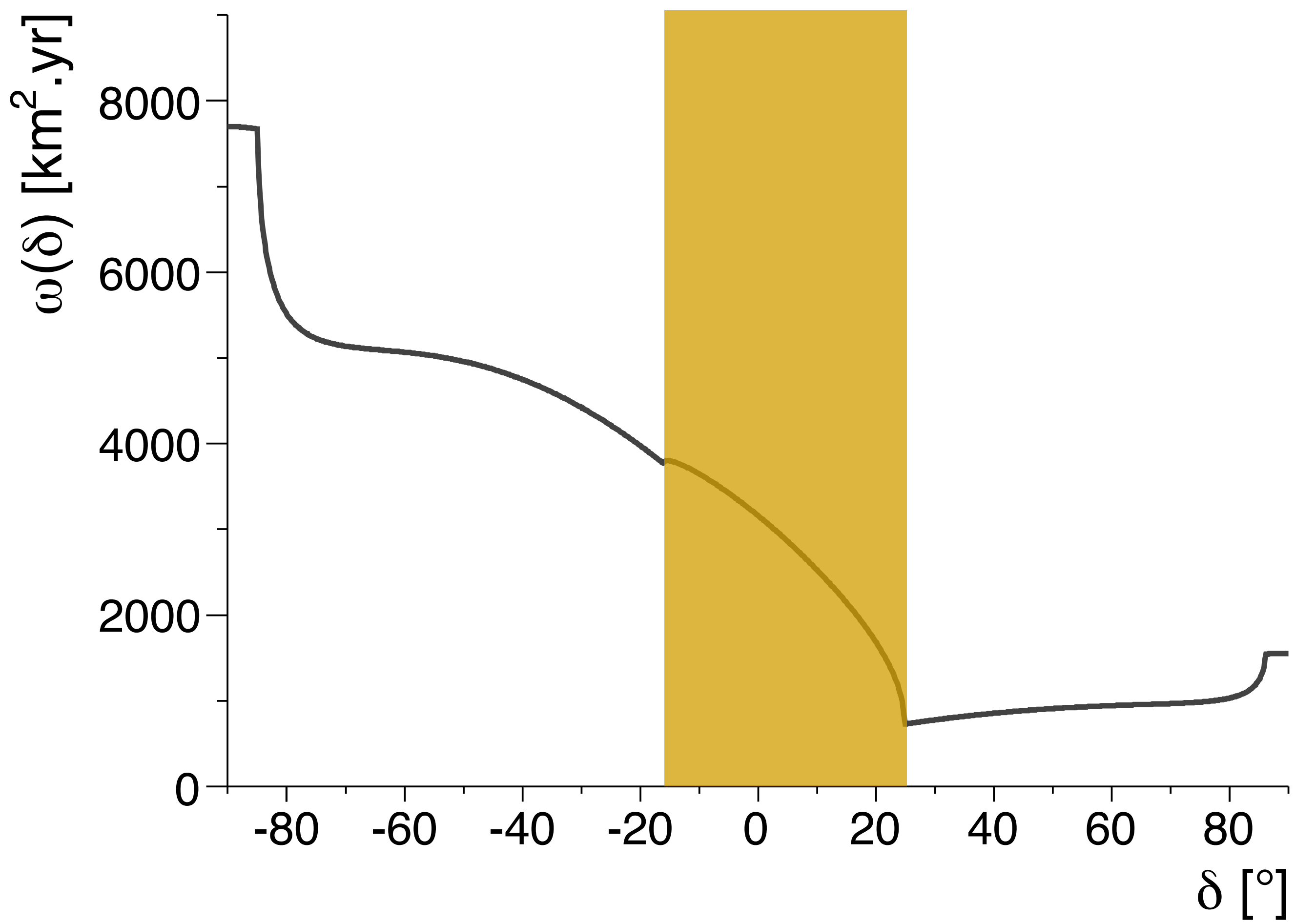

➡ BUT unavoidable uncertainty in the relative exposures of the experiments

$$\omega(\mathbf{n};b) = \omega_{\mathrm{TA}}(\mathbf{n}) + b\,\omega_{\mathrm{Auger}}(\mathbf{n}).$$

b : fudge factor absorbing systematics of any origin (relative exposure, energy scale, etc)

Full-Sky Map >10 EeV (60° smoothing)

N_{TA}~1800

(~5200 km^2 sr yr)

N_{Auger}~10900

(~32000 km^2 sr yr)

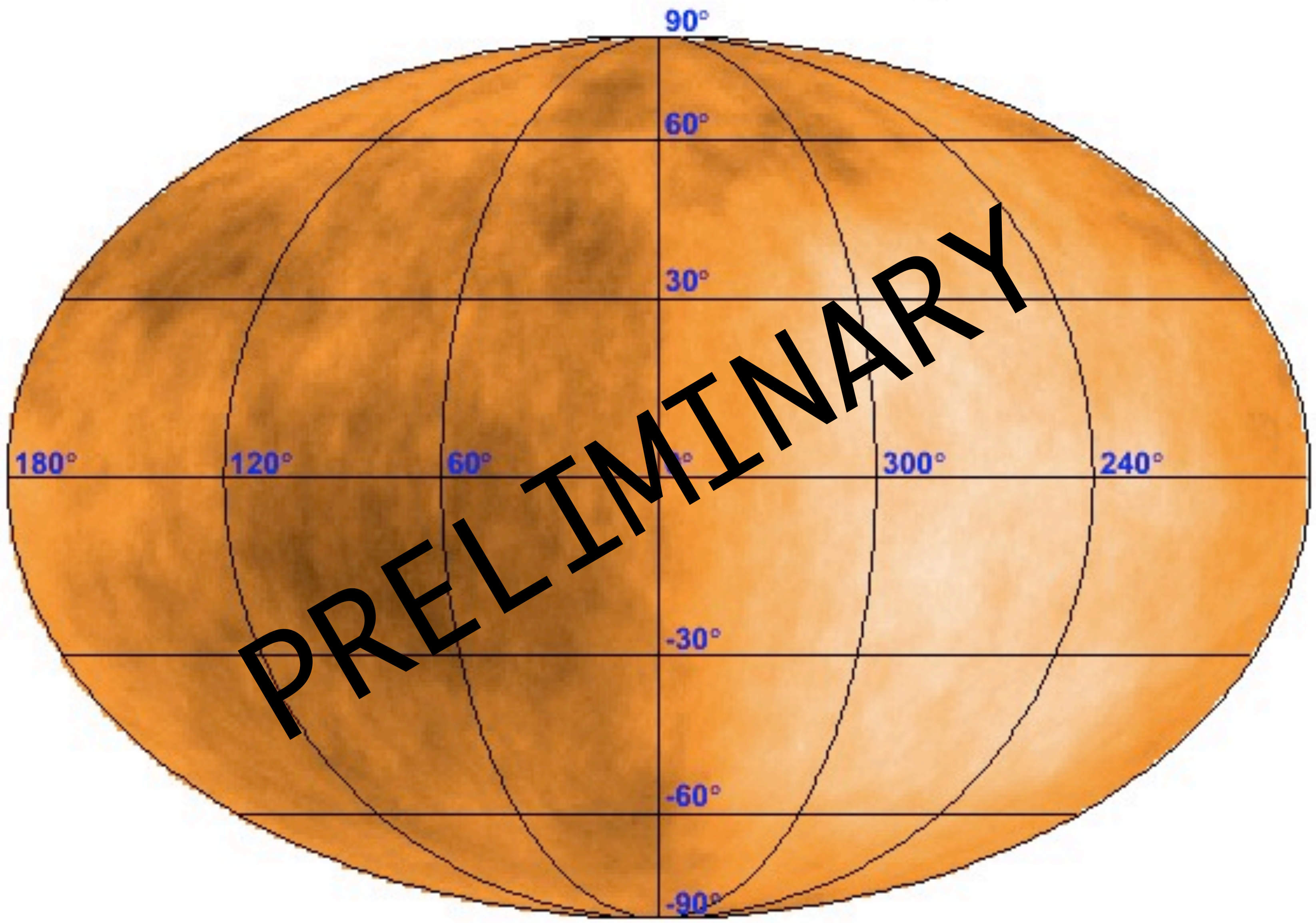

In the overlap :

N_{TA}~650

N_{Auger}~3400

Full-Sky Map >10 EeV (30° smoothing)

N_{TA}~1800

(~5200 km^2 sr yr)

N_{Auger}~10900

(~32000 km^2 sr yr)

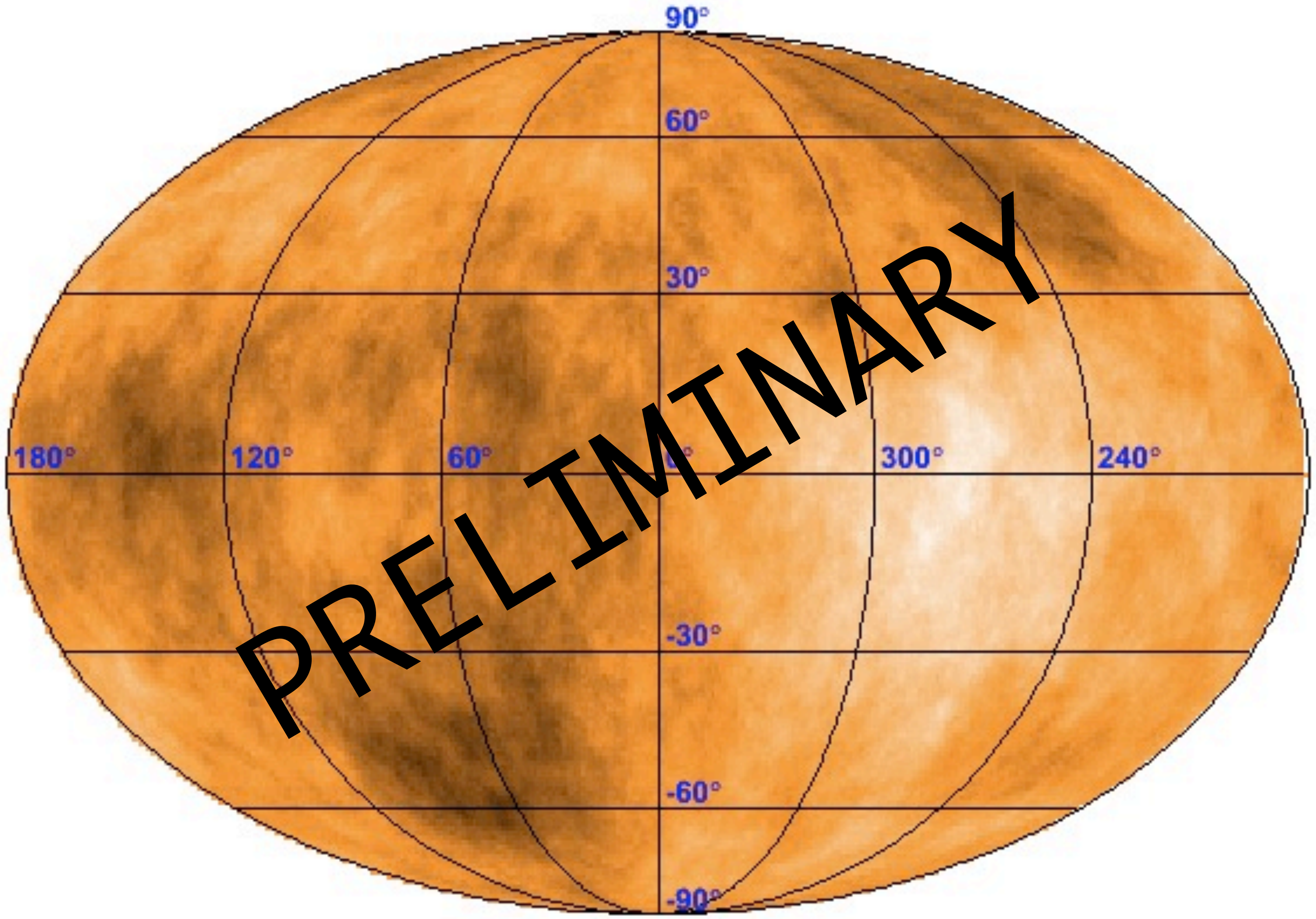

In the overlap :

N_{TA}~650

N_{Auger}~3400

SUMMARY

- Amplitudes marginally in agreement with isotropic expectations in few energy bins
- Non-random phases over a wide energy range
- Searches in both α <u>and</u> δ now possible
- Constraining upper limits on dipole/quadrupole moments
- Searches with full-sky coverage applied to Auger/TA data above 10 EeV soon
- Ongoing, searches in enriched light/heavy samples (based on event-by-event Xmax data with FD) below 1 EeV